

UNUSUAL BROAD-LINE MGII EMITTERS AMONG LUMINOUS GALAXIES IN BOSS

BENJAMIN ROIG¹, MICHAEL R. BLANTON¹, NICHOLAS P. ROSS²

Draft version March 27, 2018

ABSTRACT

Many classes of active galactic nuclei (AGN) have been observed and recorded since the discovery of Seyfert galaxies. In this paper, we examine the sample of luminous galaxies in the Baryon Oscillation Spectroscopic Survey (BOSS). We find a potentially new observational class of AGN, one with strong and broad MgII 2799Å line emission, but very weak emission in other normal indicators of AGN activity, such as the broad line H α , H β , and the near-ultraviolet AGN continuum, leading to an extreme ratio of broad H α /MgII flux relative to normal quasars. Meanwhile, these objects' narrow-line flux ratios reveal AGN narrow-line regions with levels of activity consistent with the MgII fluxes and in agreement with that of normal quasars. These AGN may represent an extreme case of the Baldwin effect, with very low continuum and high equivalent width relative to typical quasars, but their ratio of broad MgII to broad Balmer emission remains very unusual. They may also be representative of a class of AGN where the central engine is observed indirectly with scattered light. These galaxies represent a small fraction of the total population of luminous galaxies ($\simeq 0.1\%$), but are more likely (about 3.5 times) to have AGN-like nuclear line emission properties than other luminous galaxies. Because MgII is usually inaccessible for the population of nearby galaxies, there may exist a related population of broad-line MgII emitters in the local universe which are currently classified as narrow-line emitters (Seyfert 2s) or LINERs.

Subject headings: galaxies: active — galaxies: Seyfert — quasars: emission lines

1. INTRODUCTION

Astronomers have concluded that most, and possibly all, massive galaxies contain supermassive black holes at their centers. The accretion of gas onto these black holes emits light, in continuum and line emission — in such cases the black hole is referred to as an active galactic nucleus (AGN). We believe the geometry of gas and dust around AGN is complex, leading to substantially different observational signatures depending on viewing angle and other factors. In addition, the bolometric luminosity and spectrum depend strongly on the amount of fuel available for accretion.

The Eddington ratio $R_{\text{Edd}} \equiv L_{\text{bol}}/L_{\text{Edd}}$ of an AGN is a useful quantification of its activity. For luminous quasars $R_{\text{Edd}} \sim 0.1$, but at low redshift most supermassive black holes spend most of their time with much lower activity ($R_{\text{Edd}} \sim 10^{-8}$ – 10^{-3}). These low-luminosity AGN are thought to have a different physical structure and emission mechanism. In particular, given estimates of the available mass for accretion, it appears inevitable that they are radiatively inefficient, which at least partly explains their low luminosity.

At low luminosities, several studies suggest that AGN do not exhibit broad-line regions (Ho 2008). Although the effect in Ho (2008) is probably dominated by Low Ionization Nuclear Emission-line Regions (LINERs), whose status as AGN is controversial (Yan & Blanton 2012; Sarzi et al. 2010), the same effect is seen for Seyfert nuclei as well (Elitzur & Ho 2009). In addition, low luminosity AGN lack the “big blue bump” in the ultraviolet-

optical range, thought to be indicative of emission from the inner accretion disk, and are instead dominated by mid-infrared energy output. Finally, underluminous quasars exhibit the Baldwin Effect in a number of broad emission lines: the equivalent widths of these lines decrease with increasing luminosity (Baldwin 1977; Boroson et al. 1993; Thompson et al. 1999). This last trend appears consistent with the low ultraviolet-optical emission for very low luminosity AGN.

The Seyfert classification scheme, based on Balmer line widths, differentiates galaxies according to the region emitting the observed lines. Broad lines, produced in the high velocity dispersion region within a few parsecs of the black hole, are frequently obscured by a presumed dust torus surrounding the AGN. Most of the time this dusty torus completely hides the broad line region — however, sometimes the broad line region remains visible (at least partially) due to light scattering into our line of sight off of material near the AGN. However, in all cases, the narrow line region extends to 100s of parsecs, outside the dusty region of greatest obscuration. Therefore, observationally AGN fall into two rough classes, Seyfert 1 galaxies with both broad and narrow hydrogen lines, and Seyfert 2 galaxies with only narrow-line hydrogen emission.

Variations in the relative strength and visibility of the Balmer lines have led some investigators to define more detailed subdivisions of Seyferts. Seyfert 1.5 galaxies have moderate-strength broad H α and H β ; Seyfert 1.8 have weak broad H α and H β ; and Seyfert 1.9 have weak broad H α and only narrow H β (see Osterbrock & Ferland 2006; Ho 2008).

In this paper, we search the Baryon Oscillation Spectroscopic Survey (BOSS; Dawson et al. 2012) sample of target galaxies for broad MgII 2799Å emission. BOSS's

¹ Center for Cosmology and Particle Physics, Department of Physics, New York University, 4 Washington Place, New York, NY 10003

² Lawrence Berkeley National Laboratory, 1 Cyclotron Road, Berkeley, CA 94720, USA

large wavelength coverage and its target redshift distribution permits coverage of the MgII line at its 2799Å vacuum rest frame wavelength region for a large fraction of its objects.

We find a new spectral class of AGN with broad MgII $\lambda 2799\text{\AA}$ emission, but apparently extremely low near-ultraviolet continuum luminosity and broad-line Balmer emission. These galaxies appear to be even closer spectroscopically to Seyfert 2 galaxies than the Seyfert 1.9s are — with no visible broad H α or H β , but a broad component in MgII indicating AGN activity.

Section 2 describes our sample selection. Section 3 describes our comparison of these galaxies with other known AGN. Section 4 summarizes our conclusions about these objects.

2. SAMPLE SELECTION AND LINE FITTING

BOSS (Dawson et al. 2012) is part of the Sloan Digital Sky Survey III (SDSS-III; Eisenstein et al. 2011) and is designed to measure the large-scale structure of the universe by observing many luminous galaxies up to redshift $z \leq 0.8$. In the process of doing so, it takes spectra of a very large (1.5 million) sample of galaxies, allowing the discovery of unusual objects. In addition, BOSS’s observed wavelength coverage (3600 to 10400 Å) and redshift range allows us to observe the MgII $\lambda 2799$ line (as measured in the vacuum) for a much larger sample than possible with the SDSS-II target galaxy sample (which had wavelength coverage between 3800 and 9200 Å and a redshift limit $z \leq 0.6$).

We selected objects from BOSS galaxy targets observed prior to January 2011, originally picked from the v5.4.14 reductions but updated to now use the v5.4.45 spectroscopic reductions corresponding to Data Release 9 (Ahn et al. 2012). We restrict the sample to redshifts, $0.35 < z < 1.1$, for which both MgII and H β are within the BOSS spectral window (around 250,000 objects). Most of the LRGs in the BOSS data have $z < 0.8$, so extending the limit to $z = 1.1$ only adds a small number of objects.

We locate strong, broad-line MgII 2799Å emitters in these spectra by fitting a model consisting of a stellar continuum plus emission lines. The stellar continuum is composed of eleven Chabrier IMF stellar models of differing ages (13 Gyear to 0.1 Gyear), as detailed in Bruzual & Charlot (2003). We find the best-fit linear combination of these models to the observed continuum spectrum, with all non-stellar emission line regions masked. Next, we fit the residuals around each individual line region independently, with a single Gaussian model, whose width, center, and flux are allowed to vary within reasonable limits. In the region around H α , instead of independently fitting the emission lines, we fit the [NII] doublet and the H α lines simultaneously with three Gaussians. In the fits described here, we model each line with just a single Gaussian regardless of whether we expect both broad/narrow components to exist.

After we perform this fit, we select galaxies based on their MgII $\lambda 2799\text{\AA}$ properties in the v5.4.14 reductions. We select all galaxies that have a signal-to-noise ratio of at least 3.5 and $\sigma > 12\text{\AA}$ in the rest frame after de-redshifting the spectra (corresponding to a velocity dis-

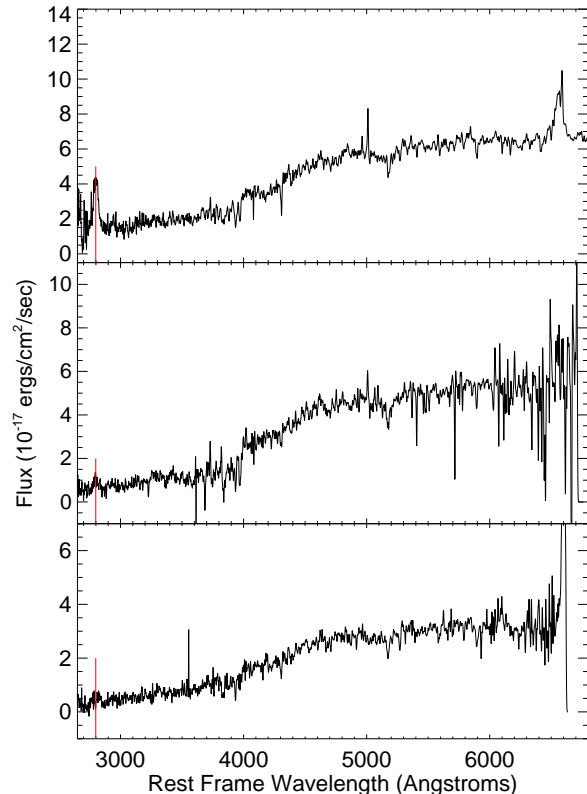


FIG. 1.— Three example BOSS target galaxies among the 293 broad-line MgII emitters, showing of the variety of spectra accepted. The spectra are smoothed but otherwise unadjusted. The three spectra are ordered by MgII line strength, with the top panel the strongest and the bottom panel the weakest. The red line indicates the wavelength of the MgII line for reference. MgII line widths vary from approximately 2000 km/s to 3000 km/s for the given objects.

persion of approximately 1300 km/s at $z = 0$). As an important note, in the update to v5.4.45, the inverse variance recorded in the spectra was decreased by approximately a factor of 2 in all spectra, rendering the criteria used for this selection inaccurate for later versions — to select a similar sample, we would need to reduce the signal-to-noise criteria by a factor of about 1.4. Finally, if the software was unable to correctly fit the MgII line in a candidate luminous galaxy, we rejected the object (indicated by the line width returning its maximum value, $\sigma = 30.0\text{\AA}$) This selection method ensures that only galaxies with real MgII detections remain in the sample — some real and weak lines may be thrown out (rejecting all objects with $\sigma = 30.0\text{\AA}$ removes about 150 objects, many of which may not have passed the visual inspection performed afterwards anyway), but the remaining sample we study will be as close to pure as possible. With these criteria, we pre-selected around 700 galaxies out of the BOSS sample.

Finally, we examined each of the spectra visually, inspecting the MgII line to see if it was a visually convincing strong line, and that the fit to the data was reasonable. If the fit was unreasonable, or the line extremely weak but broad (indicating a potential problem with continuum subtraction), we dropped the galaxy from the sample. This process eliminated about half of the previous galaxies, leaving us with a sample of 293 galaxies that show broad MgII lines that were both clearly visible

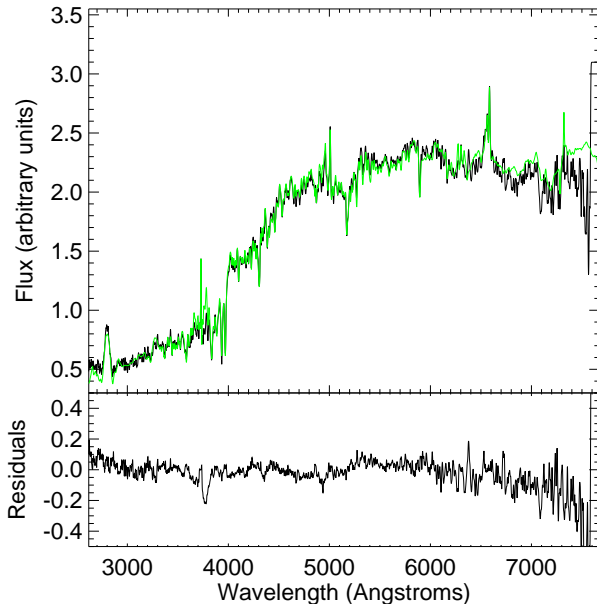


FIG. 2.— Top panel: Stack of the 162 luminous galaxies in BOSS with broad MgII detected and with wavelength coverage of both MgII $\lambda 2799\text{\AA}$ and H α ($0.35 < z < 0.57$). Our model fit to the stack is shown in green. Bottom panel: residuals of the stack minus the model.

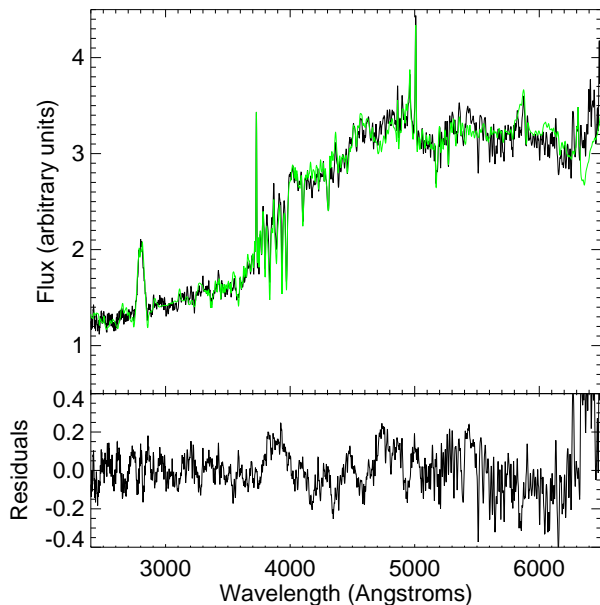


FIG. 3.— Similar to Fig. 2 for the 131 luminous galaxies with broad MgII detected but no wavelength coverage for the H α line, due to being too high redshift ($0.57 < z < 1.1$).

and well-fit by our software. Some examples of these are shown in Fig. 1 to show the varied types of MgII lines that qualified as “strong” in this paper’s sample. To better compare properties discussed later in the paper, we then split the sample in half based on redshift alone, into one set of luminous galaxies with $0.35 < z < 0.57$ (those with the H α line in the spectral coverage) and one set of luminous galaxies with $0.57 < z < 1.1$ (those without the H α line).

Because these spectra are not individually high enough signal-to-noise ratio to measure line fluxes and continuum levels precisely, we de-redshifted and stacked the

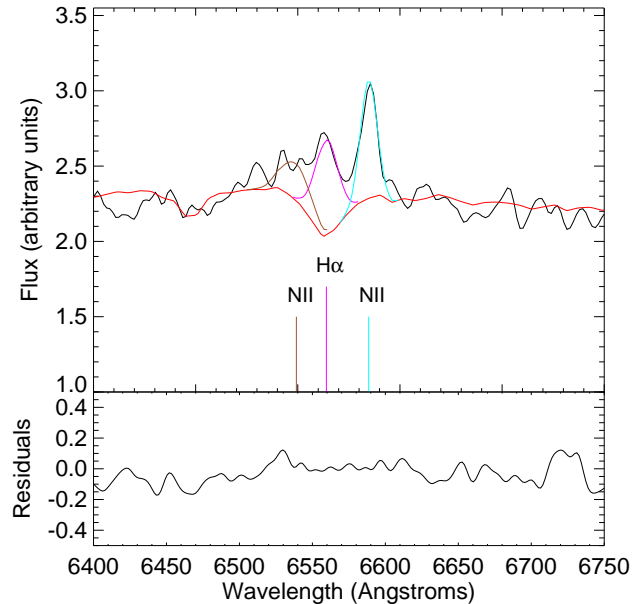


FIG. 4.— The fit from Fig. 2, zoomed in around the H α region. This plot also shows the individual gaussians used in fitting the two [NII] lines (brown and cyan) along with H α (magenta) and the base continuum flux (red). As this plot indicates, there is detected H α emission when the stellar absorption is accounted for. Although there is some overlap between the lines, we can successfully fit the complex to obtain fluxes and widths for all three lines.

two subsets of the BOSS data. The results of this stacking are shown (smoothed) as Figs. 2 and 3 in black. We fit the same model described earlier for the individual spectra to each stacked spectrum; the figures show the result in green. As the residuals show, the fitting method is successful at matching the spectra with a stellar continuum + Gaussian emission lines, with the only major discrepancies arising on the red end of the spectra.

The spectra show very strong MgII, but the other common lines expected in AGN are less obvious and only appear to contain narrow-line flux. For H β , the amount of measured flux corresponds to what would be expected based on the H α /H β ratio. However, because of the underlying stellar absorption, the line is only weakly apparent under visual inspection. The H α and [NII] complex is distinct in Fig. 2 (or for a closer view, see Fig. 4), but only the narrow components of these lines are detected (H α ≈ 250 km/s, H β ≈ 150 km/s). Finally, despite selecting strong MgII emitters that are presumed luminous galaxies hiding AGN, the ultraviolet continuum is well described by stellar continuum, without much of a rise at the blue end as a typical quasar power law model would predict.

3. WHAT TYPE OF QUASARS ARE THESE?

3.1. Are the narrow lines consistent with AGN?

With the sample of luminous galaxies selected from BOSS identified, the question now becomes “what type of quasars are these?” A first step in understanding these objects is making a BPT diagram (as in Baldwin et al. 1981) with the subset that have spectra covering H α . This is shown in Fig. 5, along with the standard theoretical divisions from Kewley et al. (2001) and Kauffmann et al. (2003). The stack falls into a Seyfert classification, though it lies rather close to the conventional dividing line between Seyferts and LINERs.

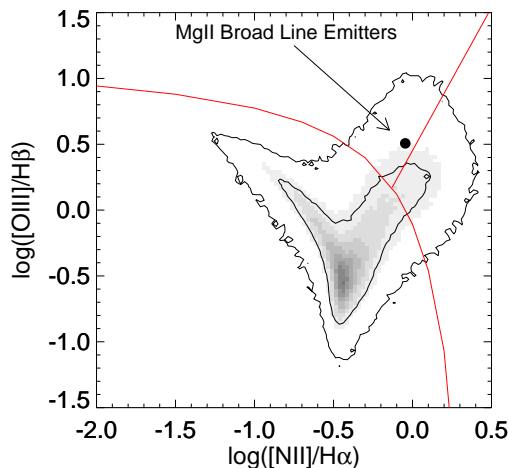


FIG. 5.— BPT diagram showing all SDSS DR8 galaxies (black background), overlaid with the stack of BOSS galaxies being considered (large black point). The uncertainties in the line ratios of the BOSS stack are approximately the size of the point. The red lines indicate the maximal star formation line dividing AGN from starforming galaxies from Kewley et al. (2001) and the empirical line dividing LINERS and Seyferts from Kauffmann et al. (2003). Our stack lies in the predicted Seyfert section, although relatively close to the division between Seyferts and LINERS.

TABLE 1
CLASSIFICATION OF BOSS TARGET GALAXIES IN THIS PAPER

	All Luminous Galaxies	MgII Emitters
Total Number	252228	293
Missing 1+ BPT Line	206849 (81.9%)	171 (58.4%)
Starbursts	26843 (10.6%)	44 (15.0%)
LINERS	13770 (5.5%)	58 (19.8%)
Seyferts	4826 (1.9%)	20 (6.8%)

NOTE. — The breakdown of the luminous galaxies in this sample, classified based on the $[\text{NII}] / \text{H}\alpha$ ratio and the $[\text{OIII}] / \text{H}\beta$ ratio. This table includes both the original set of BOSS target galaxies considered as well as the final selected sample to compare amounts of each type. It’s interesting to note that while the average luminous galaxy from our BOSS sample is classified as a Seyfert, the most common object from those with all lines present is in fact a LINER.

However, as Table 1 shows, many of the objects do not have at least one of the four lines measured, either due to low signal-to-noise in the individual spectra or redshift shifting the line out of the spectral range. For the objects with all lines, though, it’s clear that AGN-like emission (either Seyfert or LINER) is more common in these MgII emitters than in the luminous galaxy population as a whole.

3.2. Where are the broad Balmer lines?

Despite this evidence of the existence of the narrow-line region of a quasar, the $\text{H}\alpha$ line and $\text{H}\beta$ line do not appear as strong and broad as the Mg II line. In principle the broad component could be present but not easily visible. In this section we will use line ratios from SDSS quasars to predict what we expect for broad lines in our BOSS objects, and also compare various broad:narrow and broad:broad lines to search for significant discrepancies in the hope of further understanding our BOSS sample. First, to test whether these broad lines are present,

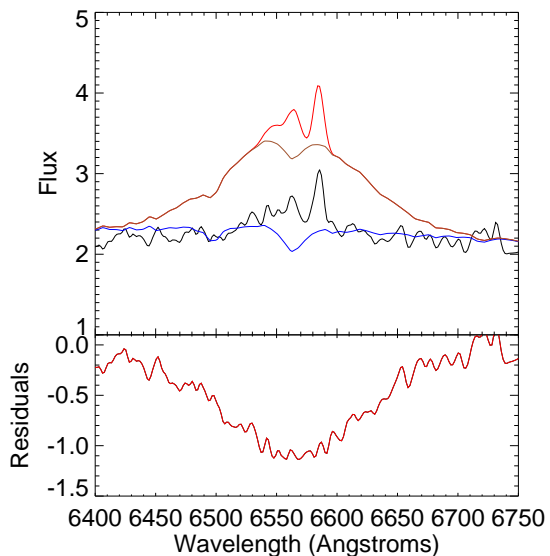


FIG. 6.— An example of what the $\text{H}\alpha$ line region would look like if our objects matched the broad $\text{H}\alpha$:MgII flux ratio found in the Shen quasar sample, as shown in Table 3, assuming the $[\text{NII}]$ lines are unchanged and the broad $\text{H}\alpha$ width is the same as our measured MgII line width. The blue line indicates the continuum level. The brown line shows the broad component and continuum, while the red is the sum of all 4 Gaussians.

we considered the set of quasars in the DR7 catalog (Shen et al. 2011) with both broad and narrow $\text{H}\alpha$ lines detected — approximately 4600 objects. Assuming that the ratio of narrow $\text{H}\alpha$ flux to broad $\text{H}\alpha$ flux is consistent in most quasars, and that the DR7 catalog has objects comparable to the ones we are considering in BOSS, we can predict what the broad $\text{H}\alpha$ flux would be in our BOSS stacked spectrum from the observed narrow-line flux. We find that on average, the SDSS quasars with both broad and narrow $\text{H}\alpha$ measured have a narrow line to broad line flux ratio of at least 1:10 in $\text{H}\alpha$. When we apply that same ratio to the observed $\text{H}\alpha$ narrow line in the AGN in our sample of luminous galaxies in BOSS, we can quickly see that the broad line emission (if present) would be clearly visible to us — and so while there may be small amounts of broad line flux present, it is certain that these objects have a much smaller ratio of broad-to-narrow $\text{H}\alpha$ than the Shen quasar sample. Fig. 6 shows what we would expect to see if we had the “proper” amount of broad $\text{H}\alpha$ in these quasars given the measured narrow $\text{H}\alpha$. The key to this is the standard $[\text{NII}]$ doublet at 6550 and 6589 Å, as the redder line in the doublet is clearly visible, forcing the blueward line to have a well-defined flux to be close to the normal ratio (approximately 3:1). However, the $[\text{NII}]$ 6550 line is weak in our sample, and this constraint on $[\text{NII}]$ 6550 strongly limits the strength of any broad feature underlying the $\text{H}\alpha$ - $[\text{NII}]$ complex.

In addition to this test, we consider how much broad $\text{H}\alpha$ we could possibly allow, to quantitatively determine how close our narrow-to-broad ratio is to that in the Shen quasar sample. We adjusted our fitting routine to fit 4 Gaussians around the $\text{H}\alpha + [\text{NII}]$ complex — one for each $[\text{NII}]$ line, and a broad and narrow $\text{H}\alpha$. Because our fit was very good to the narrow lines, we fix the

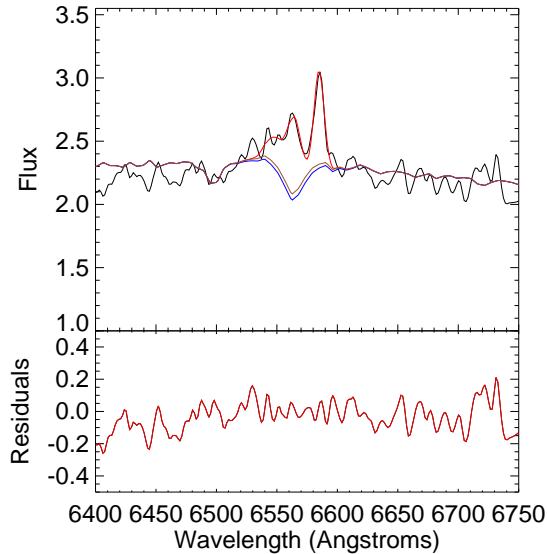


FIG. 7.— The best-fit result when we try to incorporate a broad $H\alpha$ component into our model, allowing the stellar population portion to change as needed to maximize the amount of broad $H\alpha$ that could be in the model. As is clear, very little broad $H\alpha$ is allowed in order to fit the spectrum well, despite what predictions from previously studied quasars would suggest we find. As in Fig. 6, the blue line shows the continuum, the brown the broad $H\alpha$ plus continuum, and the red the full model, and here the blue and brown lines are nearly identical.

TABLE 2
LINE RATIOS OF QUASARS AND BOSS LUMINOUS GALAXIES:
NARROW LINE:MgII FLUX RATIOS

Objects	0.35 < z < 0.57		z > 0.57
	N. $H\alpha$ /MgII	[OIII]/MgII	[OIII]/MgII
BOSS galaxies	0.306±0.01	0.280±0.007	0.244±0.006
SDSS quasars	0.458	0.149	0.091
SDSS quasars (high MgII EW)	0.160	0.113	0.112

NOTE. — These line ratios refer to spectra in Figs. 9 and 12. The first column only lists the narrow $H\alpha$ flux, not including any potential broadline components. The luminous galaxies in BOSS have, for a given MgII amount, more narrow [OIII] flux than the set of SDSS quasars, but do not follow the same pattern for narrow $H\alpha$. The subset of SDSS quasars in the last line is the set with large (> 149 Å) equivalent width in the MgII line (to be discussed in Section 3.4).

TABLE 3
LINE RATIOS OF QUASARS AND BOSS LUMINOUS GALAXIES:
BROAD $H\alpha$ FLUX RATIOS

Objects	0.35 < z < 0.57	
	Broad $H\alpha$ /MgII	Broad $H\alpha$ /Narrow $H\alpha$
BOSS LRGs	< 0.101	< 0.330
SDSS quasars	2.85	36.6
SDSS quasars (high MgII EW)	1.29	42.8

NOTE. — These line ratios refer to spectra in Figs. 9 and 12. Here we see strong discrepancies between the Shen catalog and our sample of luminous BOSS galaxies, with significantly less broad $H\alpha$ flux than would be anticipated, exacerbated since we can only accurately give an upper limit on the $H\alpha$ broadline flux. The subset of SDSS quasars in the last line is the set with large (> 149 Å) equivalent width in the MgII line (to be discussed in Section 3.4).

widths of the two [NII] Gaussians and the narrow $H\alpha$ line. Since we believe the MgII line accurately traces the broad line region as well, we fixed the width of the broad $H\alpha$ line to that value, because both lines should be produced in a similar environment. In the end, then, our fitting program only can adjust the relative amounts of flux in the four Gaussians in its attempt to model the spectrum. We find in Fig. 7 that very little broad $H\alpha$ can be hidden under the continuum.

Table 2 shows a comparison of some of the line ratios between the luminous BOSS galaxies and the SDSS quasars. We compared various narrow:broad line ratios in our BOSS objects, the full set of SDSS quasars, and the subselected set of SDSS quasars described later in Sec. 3.4. Because we already found a difference in the ratio of narrow $H\alpha$ to broad $H\alpha$, we examined whether the discrepancy persisted in other ratios. Table 2 shows a far smaller, but by no means negligible, level of discrepancy. We consistently find a modestly higher flux of [OIII] narrow-line emission relative to broad MgII (qualitatively similar to the high narrow-to-broad $H\alpha$ ratio, but a much smaller quantitative effect). We also find that considering a subset of SDSS quasars with similarly large MgII EW gives us much smaller flux ratios, as the amount of MgII flux has increased without a change in the other line on average. Based on this table, our luminous BOSS galaxies seem similar to ordinary SDSS quasars in their properties, except for their apparently very low broad $H\alpha$ flux.

However, the more interesting results come in comparing broad:broad line ratios, as Table 3 does. Here we find an extreme difference - the ratio of broad $H\alpha$ to MgII is exceptionally small in our BOSS objects compared to the Shen sample, both the selected subset and the entire sample. To show the magnitude of this, Fig. 8 shows the distribution of this ratio for all Shen objects with both lines detected (the mean and standard deviation of which are presented in Table 3). Only 7 or so objects are as extreme in this flux ratio out of the nearly 650 objects in the Shen catalog that have both lines detected, suggesting that this object is far from the norm in this ratio. Similarly when comparing the broad $H\alpha$ flux to the narrow $H\alpha$ flux, we find that the BOSS objects are quite low in comparison to the Shen sample — the ratio is about 3:1 narrow to broad rather than the 1:30 narrow to broad found from the Shen quasars. These results combined, in addition to what we visually found by fitting the spectrum in Fig 7 suggests that the broad $H\alpha$ flux is strongly suppressed, an unexpected result given how strong and broad the MgII line is.

Most notable in the results from these two tables is lack of any dramatic discrepancy between the ratios of broad MgII and narrow $H\alpha$ when compared to the SDSS quasars, combined with the large difference found between broad $H\alpha$ and narrow $H\alpha$ discussed above. Together, these results imply that the broad $H\alpha$ is very strongly suppressed even with respect to broad MgII.

3.3. Where is the continuum flux?

Next, we compared the two spectra in more detail to that of known SDSS quasars, again taken from the catalog of Shen et al. (2011). To do this, we created a “typical” SDSS quasar by splitting the quasars into the same two groups based on spectral coverage of $H\alpha$, $H\beta$,

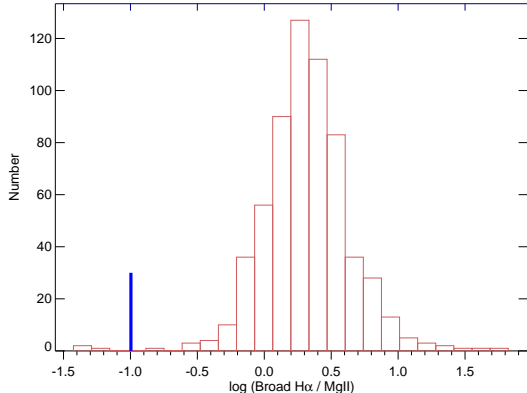


FIG. 8.— The distribution of the ratio of broad $H\alpha$ flux to $MgII$ flux for the Shen catalog, all objects that contain both recorded line fluxes. The plot is presented as the log of this value. The luminous BOSS galaxy stack we are comparing is shown with its value as a blue line at $\log(\text{broad } H\alpha/MgII) \simeq -1$, a distinct outlier.

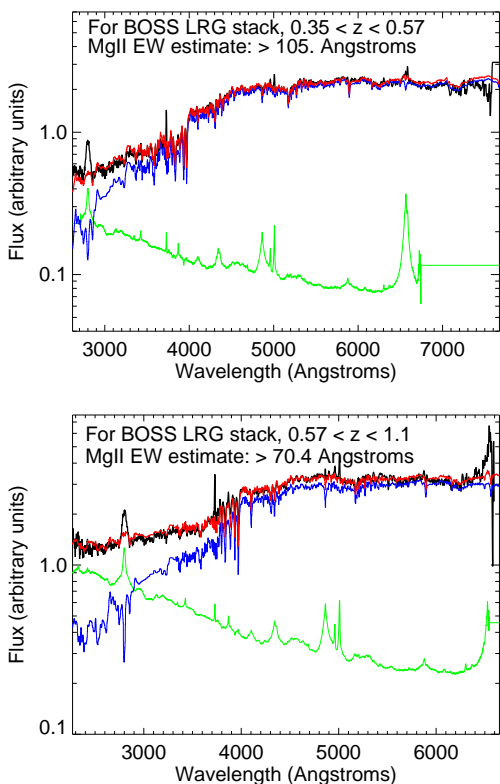


FIG. 9.— Model fit of a normal SDSS quasar and stellar continuum to luminous BOSS galaxies with broad $MgII$ in both the $0.35 < z < 0.57$ and $0.57 < z < 1.1$ redshift bins. The black line is the BOSS stack we are fitting to, the blue line indicates the stellar continuum fit to that data, and the red line is the overall model of that continuum plus the SDSS quasar component. The green line below is the maximum amount of flux from the SDSS quasar component that the model allows at 95% confidence. Based on the poor fit to the lines, these BOSS objects are extremely high $MgII$ EW and not similar to the SDSS quasars.

and $MgII$ as described previously and then stacking them (for these objects, the corresponding redshift ranges are $0.36 < z < 0.40$ and $0.40 < z < 0.90$). Because the BOSS target galaxies were identified primarily as luminous galaxies and had a strong and easily fit stellar continuum component, to best determine how much of

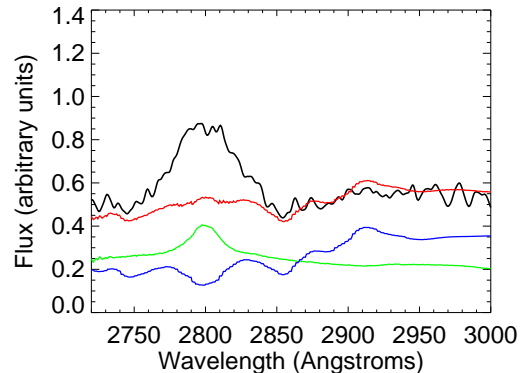


FIG. 10.— A zoomed-in view of panel 1 of Fig. 9 to show how badly the $MgII \lambda 2799\text{\AA}$ line is fit by assuming the luminous BOSS galaxy spectrum to be composed of a stellar component plus a standard SDSS quasar component. Again the black line shows the BOSS stack, the blue line is the best-fit result of the stellar continuum, and the green line indicates the 95% confidence maximum model of the quasar continuum. The red line represents the full model, the sum of the bright green and blue lines.

the flux was from the quasar component we took both the SDSS quasar stack and the stellar continuum models from earlier (shown in Figs. 2 and 3), and combined them into one 12-component model with which we refit our stacked spectra. The model parameters reveal how much continuum can be attributable to the stars in the luminous galaxy and how much can be attributable to the quasar, as well as estimate or place a limit on the equivalent width of $MgII$ relative to the quasar continuum. Fig. 9 shows these results for the $H\alpha$ and no- $H\alpha$ stacks.

The details of the quasar component of the best-fit model are not particularly well constrained, and it is better to express the results as an upper limit on the component that can be coming from a typical quasar. To do so, we evaluated the 95% confidence limit based on the increase in χ^2 as we increased the quasar amplitude. This limit is shown as the green line in Figure 9.

These figures suggest that these luminous galaxies, despite their broad $MgII$ emission, do not have typical quasar spectra. The ultraviolet continuum in Figure 10 is sufficiently well-explained by the stellar emission such that the much bluer quasar continuum is forced to low amplitude in our best-fit model (the vertical scale is logarithmic in these figures).

Spectrophotometric calibration is a potential concern; the systematic uncertainties in the ultraviolet due to calibration are likely to be larger than the statistical errors. To test for such issues, we also attempted modeling the stacked spectra with the 12 components described above, and two additional components, one constant and one linear in wavelength, to allow the spectrum to tilt a bit. While this did indeed produce a somewhat better fit with a greater contribution from the quasar model, it also required that we have fluxing errors on the order of a factor of two at the blue end of the spectrum (below 4000\AA mostly), far more than should be expected in these spectra (around 10% at most).

3.4. What do the continuum limits tell us?

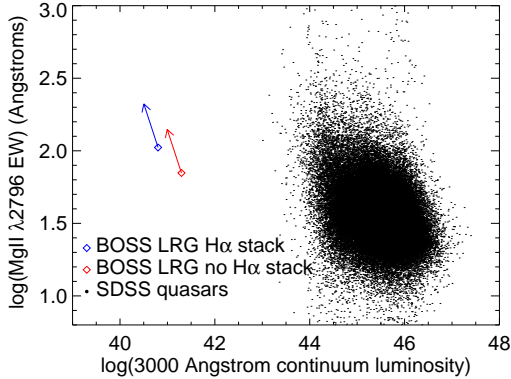


FIG. 11.— Given the 95% confidence fits in Fig. 9, this plot shows the limits on the MgII equivalent width in the luminous BOSS galaxies relative to the SDSS quasars. The SDSS quasars exhibit the Baldwin Effect, a decrease in the equivalent width as a function of quasar luminosity. As expected, the luminous BOSS galaxy stacks are high EW, which may be related to their low luminosity. Indeed, they lie roughly along the predicted path of lower continuum luminosity and higher EW. The two points shown are the stacks in the redshift range $0.35 < z < 0.57$ (blue) and $0.57 < z < 1.1$ (red).

Now noting that the AGN portion of the continuum is apparently very low, we wanted to see if the large MgII flux is possibly an extension of the Baldwin Effect as described in Baldwin (1977) in an extreme case of very low continuum. We calculate the equivalent width (EW) of the MgII $\lambda 2799\text{\AA}$ line by using the line flux found in our line fitting procedure from earlier, and take the 95% confidence maximum quasar continuum as our continuum value. Fig. 11 shows that the luminous BOSS galaxies are indeed low continuum and high MgII flux. Because our measurement of the AGN continuum is an upper limit, we show the luminosity and EW in this plot as a 95% confidence limit. Thus, although these luminous galaxies are certainly not similar spectroscopically to the Shen catalog of SDSS quasars, they do following a known trend for quasars and are conceivably just an extreme but not unknown case.

To further examine this comparison of large MgII EW quasars to our BOSS galaxies, we then selected the subset of quasars from the Shen catalog that have large MgII equivalent widths, potentially the closest subset to the luminous BOSS galaxies we are examining. Few are as extreme as the luminous BOSS galaxies in both EW and luminosity, but if our objects are best compared to quasars with large MgII EW, then performing the same fit from before with only large MgII EW SDSS quasars should result in a better match for both the continuum and emission lines. This alternative fit is shown as Fig. 12. Here we see progress in matching the spectra, especially in the bottom panel where our model seems to explain the data relatively well, but note that the top panel still shows a significant MgII flux deficit, suggesting that possibly our objects require the most extreme MgII EW quasars to be explained. Also of note is that this subset of quasars still does not address the issues around the missing broad H α . Other subsets of the Shen catalog were considered (objects with small broad H α /MgII ratio, objects with low Eddington ratio, and objects with the broadest MgII lines), but none of these approaches led to improved fit

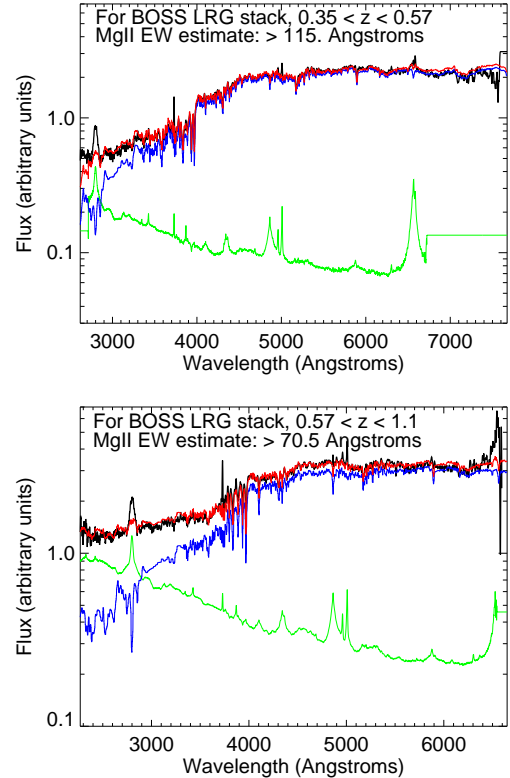


FIG. 12.— Similar to Fig. 9, but only stacking SDSS quasars with large ($> 149\text{\AA}$) MgII EW. In this case, one of our two stacks has a better fit model (the bottom panel), while the other still remains a poor fit.

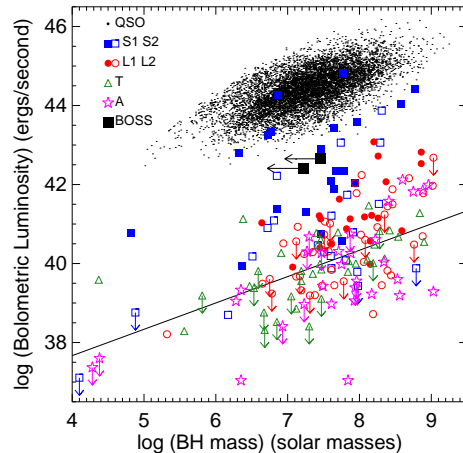


FIG. 13.— Comparison of the BOSS galaxies with broad MgII to the black hole masses and bolometric luminosity data presented in Elitzur & Ho (2009). As labeled, the colors are the same as their original plots, with the 2 stacks of luminous BOSS galaxies overlaid as black points. The maximum BH mass is calculated given the maximum continuum fit in Fig. 9 and represents an upper limit. The uncertainty in the bolometric luminosity is from the uncertainty in the [OIII] line fit, and is approximately the size of the data point.

qualities in any of the lines or continuum regions.

3.5. Should we expect a broad line region?

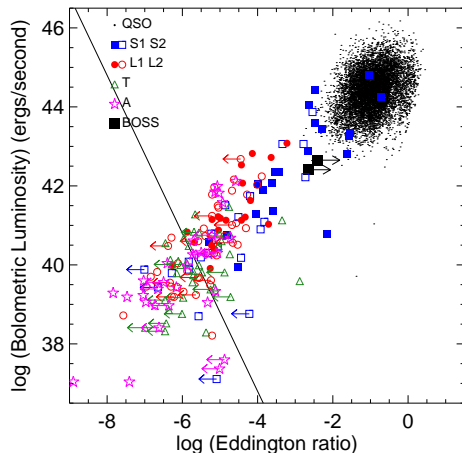


FIG. 14.— Comparison of the BOSS galaxies to the Eddington ratios and bolometric luminosities presented in Elitzur & Ho (2009). As labeled, they are the same as their original plots, with the 2 stacks of luminous BOSS galaxies overlaid as black points. The minimum Eddington ratio is calculated given the maximum continuum fit in Fig. 9 and represents a lower limit. The uncertainty in the bolometric luminosity is from the uncertainty in the [OIII] line fit, and is approximately the size of the data point.

The broad line regions in these luminous galaxies appear unusual, with a very low broad-line flux in the Balmer lines; in addition, the AGN have a remarkably low continuum. Elitzur & Ho (2009) found that given a BH mass, there was a bolometric luminosity below which no broad-line regions were found in the $H\alpha$ and $H\beta$ lines. The question arises whether, given the result of Elitzur & Ho (2009) and the observed narrow-line fluxes, we should have expected our MgII emitting luminous galaxies to have broad-line regions, or whether Elitzur & Ho (2009) would have predicted no broad line region.

To do so, we use the MgII line and 3000\AA continuum luminosity to estimate a black hole (BH) mass, following the prescription given in Wang et al. (2009). Our 3000\AA continuum luminosity is obtained from the 95% confidence maximum quasar continuum in the fits displayed in Fig. 9. This procedure yields an upper limit on the BH mass. Once the BH mass is obtained, we calculate its Eddington luminosity. Finally, we derive a bolometric luminosity from the [OIII] $\lambda 5007\text{\AA}$ line using the relation derived in Heckman et al. (2004), and then compute the Eddington ratio used in Figure 1 of Elitzur & Ho (2009). Note that as these measurements were derived from a 95% confidence continuum, they correspond to a maximal BH mass and a minimum Eddington ratio respectively, and are plotted as limits rather than data points. Figs. 13 and 14 reproduce Figure 1 from Elitzur & Ho (2009) with our data added as large black points, with arrows showing the direction of the minimal/maximal uncertainties explained above.

All these estimates are made on the basis of the MgII line because the other, more commonly used lines are much weaker. Based on our findings above, these objects are unusual, and therefore the black hole masses and Eddington ratios estimates may be incorrect. In fact, we present some evidence for these black holes masses being somewhat underestimated below. Nevertheless,

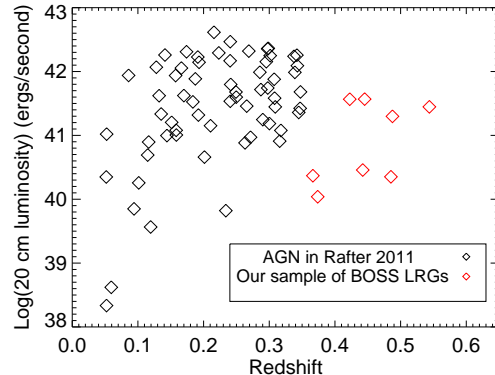


FIG. 15.— The redshift-radio luminosity plot showing our sample of luminous BOSS galaxies with detectable radio emission in FIRST along with the sample discussed in Rafter et al. (2011). Our objects sit at higher redshift, indicating the possibility that the very limited detections were due to flux limits, but this plot suggests that this is not the case as we do not find the highest brightness radio sources anywhere in our 293 galaxies as in the Rafter sample, which we would expect if our galaxies were also BLRGs.

given the bolometric luminosities from [OIII], the black hole masses would have to be larger than any known black holes in the universe to violate the relation given in Elitzur & Ho (2009).

These results suggest that the broad-line regions in these luminous galaxies are safely consistent with the luminosity limits presented in Elitzur & Ho (2009). However, it is notable that these luminous galaxies are missing this BLR evidence in $H\alpha$ and $H\beta$, which for most local samples are the only accessible lines. It is possible that some galaxies in the local Universe currently classified as Seyfert 2s actually house a detectable MgII region — potentially even some of those below the threshold determined in Elitzur & Ho 2009.

3.6. Radio properties

Here we investigate the radio properties of our sample galaxies, and compare to typical broad-line radio galaxies (BLRGs). Rafter et al. (2011) investigated radio properties of confirmed broadline AGN in SDSS in an attempt to correlate radio loudness with other properties. To compare our sample with theirs, we searched the FIRST catalog for objects in our sample with FIRST detections. Very few objects appeared in both — only 4 distinct objects of the 293 had matches in FIRST within 0.5 arcseconds that were brighter than 3 mJy integrated radio flux. Four other objects were found with very weak radio flux and are also included, but they are barely above the detection limit — clearly not strong radio emitters. Despite several similar optical spectra, our sample does not appear to be similar to the BLRGs discussed in Rafter et al. (2011) on the whole.

However, it is worth noting that the objects that do have radio detections are of similar luminosities as the sample in Rafter et al. (2011). Fig. 15 shows both sets of objects plotting redshift versus luminosity. Since our objects are higher redshift, it is possible that the reason fewer are detected was a selection effect in FIRST; this appears to not be the case, however, because we are missing objects in the high luminosity range as well. Although our objects may end up being physically similar

to typical BLRGs, they are typically lower radio luminosity.

3.7. Position relative to the $M_{\text{BH}}-\sigma$ relation

As a comparison to other black holes, we can place these stacked objects from BOSS on the relationship between black hole mass and stellar velocity dispersion. However, not every one of the luminous galaxies has a recorded stellar velocity dispersion, so our data needed some slight modification. To avoid biasing the estimated black hole mass due to a systematic reason for an unmeasurable stellar velocity dispersion, for this plot we added one more cut before stacking the objects, measuring line and continuum fluxes, and calculating a black hole mass. This new cut removed all objects that did not have an estimated stellar velocity dispersion — although this is a small percentage of the total objects we kept, it has a non-negligible effect on the upper limit BH mass estimate. Fig. 16 shows where our objects lie, with the caveat as previously mentioned that we can only estimate an upper limit on the black hole masses due to the very weak AGN continuum.

Fig. 16 suggests quite strongly that for these luminous BOSS galaxies, the standard prescriptions (such as that of Wang et al. 2009) for deriving a black hole mass from MgII do not work well. However, it is important to note that these values assume we are seeing the entire flux from the relevant lines. In section 3.9, we will note that perhaps our objects have scattered broad line flux and are not seen directly, and perhaps these estimates are too low for that reason. By not seeing the broad line region directly, we may not see the entirety of the MgII flux that is produced, and so our estimates depending on the fluxes in any broad lines could be underestimates. For normal (viewed directly) objects, MgII provides consistent (with $\text{H}\alpha$) BH masses (see Matsuoka et al. 2013; Onken & Kollmeier 2008; McGill et al. 2008). However, in our sample we find much smaller black hole masses than the $M-\sigma$ relation predicts. If the MgII line remains accurate as a BH mass indicator in these objects, they fall below the typical masses given the velocity dispersions of the galaxies, by much more than the scatter in the relationship.

3.8. Dust properties in the narrow line region

For the subset of the luminous galaxies in this sample observed between redshifts 0.35 and 0.57, we can calculate the Balmer decrement in the narrow-line fluxes, to estimate the degree of interstellar reddening of the narrow-line region. A very reddened narrow-line region would be suggestive of an unusual geometry or very dusty system, which might allow us to attribute the lack of broad Balmer lines to these properties of the system as well (though it would still be unusual that MgII was not even more extinguished). Typical Seyfert galaxies have a Balmer decrement $\text{H}\alpha/\text{H}\beta \sim 3-4$ (Osterbrock & Ferland 2006) and for our objects we find a Balmer decrements of 3.86 ± 0.21 . Figure 17 shows the distribution of Balmer decrements for typical SDSS quasars; the BOSS objects are near the median of from this distribution. Of course, the fact that the narrow-line region is not unusually affected by dust does not rule out that the broad-line region still might be.

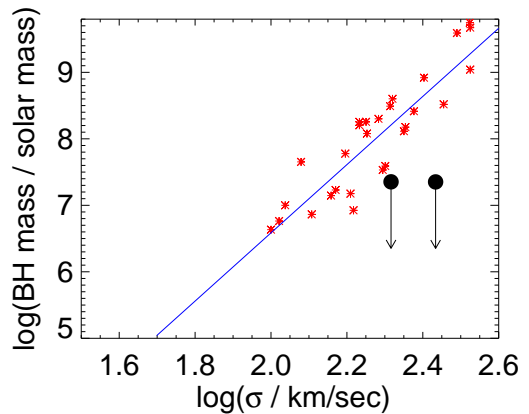


FIG. 16.— Our data relative to the $M_{\text{BH}}-\sigma$ relation, with our estimated upper limit for the black hole mass plotted as large black circles. Data from Graham et al. (2011) is shown in red along with the best-fit line from the same paper in blue. Our objects are at best on the low end of the distribution, even given the intrinsic spread, and potentially much lower depending on the exact AGN continuum level. Either these black holes are extraordinarily low mass relative to their host galaxies, or existing relations between the MgII $\lambda 2796\text{\AA}$ line and black hole mass are flawed for objects like ours.

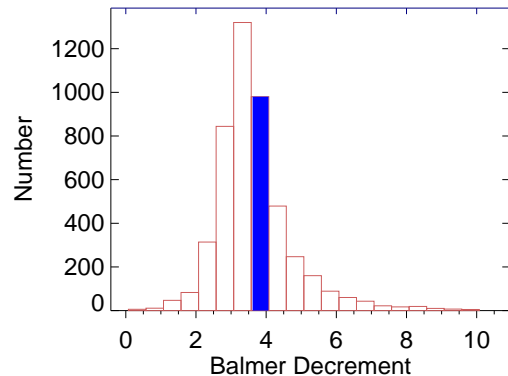


FIG. 17.— The distribution of Balmer decrements for all SDSS quasars from the Shen catalog that have both $\text{H}\alpha$ and $\text{H}\beta$ detected. (approx. 4800 quasars). The majority are around a value of 3-4, and the Balmer decrement for the BOSS stack is indicated as at the location of the blue bin. The luminous BOSS galaxy stack's Balmer decrement does not differ from the standard Balmer decrement seen in many quasars.

3.9. Scattering and polarization in the broad line region

In the previous section, we noted that no dust reddening was apparent in the narrow-line region. However, as we do not have any visible broad line $\text{H}\alpha$ or $\text{H}\beta$, we cannot make the same conclusion for the broad line region. It is possible that these objects have a geometry where there is a cloud (internal to the narrow line region, but external to the broad line region) obscuring the broad line region from our direct line of sight. Then, the broad lines we observe could be scattered instead of in direct line of sight of us, while the narrow line emission is unchanged. Objects like this have been observed in the past — see Schmidt et al. (2002, 2007); di Serego Alighieri et al. (1996) among many others recording spectra of these rare but known objects.

Many quasars hidden in galaxies exhibit flat quasar spectra (see especially di Serego Alighieri et al. (1996)) with prominent narrow lines. This is in contrast to a di-

rectly viewed, very luminous quasar, which have a power law shape to their continua, but similar to our observed objects (see Fig. 9). At the least, we cannot rule out a flat quasar spectrum to the same degree we can a standard luminous quasar spectrum — objects such as those presented in the above papers would be better fits to our spectra. Unfortunately, none of these previously studied objects have the spectral coverage for both MgII and H α , so we are unable to compare the broad line fluxes in both simultaneously. While none of them have such a strong galaxy component in their spectra, the quasar portions of the spectra are potentially very similar.

This flat spectrum can actually be hiding a more standard quasar spectrum in polarized light, as seen in IRAS 09104+4109 (discussed in several papers: see Hines & Wills (1993) and Hines et al. (1999) for details). This object’s unpolarized continuum is nearly flat between 2500 and 6500 Å, but when the polarized flux is examined the object reveals a clear quasar continuum with standard power law slope. It’s quite possible that our objects resemble this, although we cannot confirm that without spectropolarimetry. The most important characteristic of IRAS 09104+4019 is that it, like our objects, had no broad line emission recorded in the Balmer lines in the initial detections in Kleinmann et al. (1988) — as the MgII line was not observed due to wavelength coverage — until it was re-observed with broader band spectrophotometry by Hines and Wills. These followup observations showed similar broad MgII emission to our objects. As IRAS 09104+4109 was eventually found to have broad Balmer line emission in a polarized spectrum, further investigation of our objects with spectropolarimetry may be useful to see if similarities persist.

If the MgII line is being seen via scattered light, and our quasars remain normal in terms of H α emission line production, then the efficiency of the scattering of H α must be very low relative to that of MgII. We see a large MgII flux already and no definitive broad H α — so the scattering properties must be such to emphasize this discrepancy (perhaps similar to those in IRAS 09104+4019).

It would be very valuable to examine some of the strongest examples of these objects using spectropolarimetry to see if the MgII line is polarized as this hypothesis would predict, and to confirm the narrow lines are unpolarized as well, as observed in IRAS 09104+4109.

4. SUMMARY

We have found a set of luminous galaxies in BOSS that exhibit unusual properties related to the MgII λ 2799Å line. Specifically we reach the following conclusions:

1. This sample of galaxies has clear broad MgII line emission, but a much smaller broad H α flux ratio relative to MgII than typical for luminous quasars (by a factor of a few tens).
2. This sample of galaxies have narrow Balmer line fluxes and [OIII] flux ratios relative to MgII that are roughly typical for luminous quasars (within a factor of two or three).
3. Galaxies with this property are an extremely small subset of the BOSS sample ($< 0.1\%$).

4. The continuum flux from the AGN in these luminous galaxies is undetectably low, which means they must have a large equivalent width in the MgII line (possibly consistent with the Baldwin Effect seen for more luminous quasars).
5. Given the $M_{\text{BH}}-\sigma$ relation, either the MgII based black hole mass indicators used for more luminous quasars do not work for these lower luminosity objects, the black holes in these galaxies are small with respect to the expected mass given their host galaxy, or the light from the BLR is scattered such that we only see a fraction of the MgII emission.
6. The galaxies appear to be low Eddington ratio ($< 10^{-2}$) given the expected black hole mass.

The physical nature of these objects is unclear. Their lack of low continuum flux may be related to whatever physical cause lies behind the Baldwin Effect, which is itself still under debate. Given how uncommon these galaxies are, some unusual configuration around the black hole may allow obscuration of the continuum but not the broad-line region. Many ideas have been proposed to explain how these and other causes could contribute to the Baldwin effect (see Green et al. 2001 for a discussion), such as disk inclination, luminosity-dependent spectral energy distributions, or changing optical thickness of clouds around the black hole, and it is possible that one or more of these may be at play in our sample.

Why the broad-line Balmer emission remains so weak is also unknown. Differences of this objects from luminous quasars in metallicity or relative ionization fractions are unlikely to cause as large a difference in flux ratios as we observe. We can only offer up the wavelength-dependent scattering of the broad-line region as a possible explanation as to why the broad Balmer lines could be missing and the broad MgII line so strong.

Among known Seyfert 2 galaxies of lower stellar mass than these luminous galaxies, very few have had their rest-frame MgII 2799 Å region observed, because the vast majority of known galaxies are at low redshift and MgII is too blue to be observed. The population of broad-line galaxies found here may exist in lower luminosity galaxies as well, in lesser or greater abundance than found for the luminous BOSS galaxies. Therefore, some fraction of galaxies currently classified as Seyfert 2s may have broad-line regions that are observable, but only in the as-yet-unobserved MgII line.

We thank Renbin Yan and Mike Eracleous for useful conversations during the preparation of this paper. This work was partially supported by nsf-ast 12211644 and NSF-AST-0908354.

We would also like to thank the referee for his very helpful comments, especially directing us towards the class of AGN observed via scattered light.

Funding for SDSS-III has been provided by the Alfred P. Sloan Foundation, the Participating Institutions, the National Science Foundation, and the U.S. Department of Energy Office of Science. The SDSS-III web site is <http://www.sdss3.org/>.

SDSS-III is managed by the Astrophysical Research Consortium for the Participating Institutions of the SDSS-III Collaboration including the University of Arizona, the Brazilian Participation Group, Brookhaven National Laboratory, University of Cambridge, Carnegie Mellon University, University of Florida, the French Participation Group, the German Participation Group, Harvard University, the Instituto de Astrofísica de Canarias, the Michigan State/Notre Dame/JINA Participa-

tion Group, Johns Hopkins University, Lawrence Berkeley National Laboratory, Max Planck Institute for Astrophysics, Max Planck Institute for Extraterrestrial Physics, New Mexico State University, New York University, Ohio State University, Pennsylvania State University, University of Portsmouth, Princeton University, the Spanish Participation Group, University of Tokyo, University of Utah, Vanderbilt University, University of Virginia, University of Washington, and Yale University.

REFERENCES

- Ahn, C. P., Alexandroff, R., Allende Prieto, C., Anderson, S. F., Anderton, T., Andrews, B. H., Aubourg, É., Bailey, S., Balbinot, E., Barnes, R., & et al. 2012, *ApJS*, 203, 21
- Baldwin, J. A. 1977, *ApJ*, 214, 679
- Baldwin, J. A., Phillips, M. M., & Terlevich, R. 1981, *PASP*, 93, 5
- Borson, T. A., Salzer, J. J., & Trotter, A. 1993, *ApJ*, 412, 524
- Bruzual, G. & Charlot, S. 2003, *MNRAS*, 344, 1000
- Dawson, K. S. et al. 2012, *ArXiv e-prints*
- di Serego Alighieri, S., Cimatti, A., Fosbury, R. A. E., & Perez-Fournon, I. 1996, *MNRAS*, 279, L57
- Eisenstein, D. J., Weinberg, D. H., Agol, E., Aihara, H., Allende Prieto, C., Anderson, S. F., Arns, J. A., Aubourg, É., Bailey, S., Balbinot, E., & et al. 2011, *AJ*, 142, 72
- Elitzur, M. & Ho, L. C. 2009, *ApJ*, 701, L91
- Graham, A. W., Onken, C. A., Athanassoula, E., & Combes, F. 2011, *MNRAS*, 412, 2211
- Green, P. J., Forster, K., & Kuraszekiewicz, J. 2001, *ApJ*, 556, 727
- Heckman, T. M., Kauffmann, G., Brinchmann, J., Charlot, S., Tremonti, C., & White, S. D. M. 2004, *ApJ*, 613, 109
- Hines, D. C., Schmidt, G. D., & Smith, P. S. 1999, *ApJ*, 514, L91
- Hines, D. C. & Wills, B. J. 1993, *ApJ*, 415, 82
- Ho, L. C. 2008, *ARA&A*, 46, 475
- Kauffmann, G., Heckman, T. M., Tremonti, C., Brinchmann, J., Charlot, S., White, S. D. M., Ridgway, S. E., Brinkmann, J., Fukugita, M., Hall, P. B., Ivezić, Ž., Richards, G. T., & Schneider, D. P. 2003, *MNRAS*, 346, 1055
- Kewley, L. J., Dopita, M. A., Sutherland, R. S., Heisler, C. A., & Trevena, J. 2001, *ApJ*, 556, 121
- Kleinmann, S. G., Hamilton, D., Keel, W. C., Wynn-Williams, C. G., Eales, S. A., Becklin, E. E., & Kuntz, K. D. 1988, *ApJ*, 328, 161
- Matsuoka, K., Silverman, J. D., Schramm, M., Steinhardt, C. L., Nagao, T., Kartaltepe, J., Sanders, D. B., Treister, E., Hasinger, G., Akiyama, M., Ohta, K., Ueda, Y., Bongiorno, A., Brandt, W. N., Brusa, M., Capak, P., Civano, F., Comastri, A., Elvis, M., Ho, L. C., Lilly, S. J., Mainieri, V., Masters, D., Mignoli, M., Salvato, M., Trump, J. R., Taniguchi, Y., Zamorani, G., Alexander, D. M., & Lin, Y.-T. 2013, *ArXiv e-prints*
- McGill, K. L., Woo, J.-H., Treu, T., & Malkan, M. A. 2008, *ApJ*, 673, 703
- Onken, C. A. & Kollmeier, J. A. 2008, *ApJ*, 689, L13
- Osterbrock, D. E. & Ferland, G. J. 2006, *Astrophysics of gaseous nebulae and active galactic nuclei*
- Rafter, S. E., Crenshaw, D. M., & Wiita, P. J. 2011, *AJ*, 141, 85
- Sarzi, M., Shields, J. C., Schawinski, K., Jeong, H., Shapiro, K., Bacon, R., Bureau, M., Cappellari, M., Davies, R. L., de Zeeuw, P. T., Emsellem, E., Falcón-Barroso, J., Krajnović, D., Kuntschner, H., McDermid, R. M., Peletier, R. F., van den Bosch, R. C. E., van de Ven, G., & Yi, S. K. 2010, *MNRAS*, 402, 2187
- Schmidt, G. D., Smith, P. S., Foltz, C. B., & Hines, D. C. 2002, *ApJ*, 578, L99
- Schmidt, G. D., Smith, P. S., Hines, D. C., Tremonti, C. A., & Low, F. J. 2007, *ApJ*, 666, 784
- Shen, Y., Richards, G. T., Strauss, M. A., Hall, P. B., Schneider, D. P., Snedden, S., Bizyaev, D., Brewington, H., Malanushenko, V., Malanushenko, E., Oravetz, D., Pan, K., & Simmons, A. 2011, *ApJS*, 194, 45
- Thompson, K. L., Hill, G. J., & Elston, R. 1999, *ApJ*, 515, 487
- Wang, J.-G., Dong, X.-B., Wang, T.-G., Ho, L. C., Yuan, W., Wang, H., Zhang, K., Zhang, S., & Zhou, H. 2009, *ApJ*, 707, 1334
- Yan, R. & Blanton, M. R. 2012, *ApJ*, 747, 61